Modeling of the Effect of Multiple Scattering in Photon Correlation Spectroscopy: Plane-Wave Approach

Vladimir I. Ovod

Met One, Inc., 481 California Avenue, Grants Pass, Oregon 97526, and Department of Chemistry, University of California, Santa Barbara, California 93106

Daniel W. Mackowski

Department of Mechanical Engineering, Auburn University, Alabama 36849

Robert Finsy

Department of Theoretical Physical Chemistry, Vrije Universiteit Brussel, Pleinlaan 2, B-1050 Brussels, Belgium

Langmuir®
The ACS Journal of Surfaces and Colloids

Reprinted from
Volume 14, Number 10, Pages 2610–2618

Articles

Modeling of the Effect of Multiple Scattering in Photon Correlation Spectroscopy: Plane-Wave Approach

Vladimir I. Ovod*

Met One, Inc., 481 California Avenue, Grants Pass, Oregon 97526, and Department of Chemistry, University of California, Santa Barbara, California 93106

Daniel W. Mackowski

Department of Mechanical Engineering, Auburn University, Alabama 36849

Robert Finsy

Department of Theoretical Physical Chemistry, Vrije Universiteit Brussel, Pleinlaan 2, B-1050 Brussels, Belgium

Received December 27, 1996. In Final Form: December 11, 1997

A technique for numerical modeling of the time autocorrelation function (ACF) of the electric field scattered from a concentrated dispersion, which is illuminated by a plane wave, has been developed as an approach to estimate the particle dynamics and multiple scattering effects in photon correlation spectroscopy measurements. Systematic error of the modeling of the particle dynamics and the error of the ACF estimation were investigated for Brownian free particles. It has been found that systematic error and the decreased dynamic delay-time range of the ACF exponential behavior for free particles are caused by low- and high-frequency oscillations of integrated functions. An optimization of the numerical model has been carried out in order to reach a required magnitude of the systematic error and a maximum of the dynamic delay-time range by a minimum of calculation expenditures. The dynamics of an ensemble of particles was generated by a stochastic technique. Practical application of the proposed technique was shown by modeling of the first-order ACF for the depolarized component of the backscattered electric field. Influence of multiple-scattering by interacting spheres on this ACF was investigated for different sphere diameters and dispersion concentrations by using a rigorous multiple-scattering technique. This model can be used to further develop photon correlation spectroscopy for the characterization of particles in concentrated and turbid media: in a following paper, the multiple-scattering suppression by one-beam cross correlation is simulated, taking into account geometrical parameters of a setup.

1. Introduction

Photon correlation spectroscopy (PCS) is a powerful tool for the on-line particle sizing in variety-dispersed systems.[1,2] PCS is based on the measurement of the normalized intensity autocorrelation function (ACF):

$$g^{(2)}(\tau) = \frac{G^{(2)}(\tau) - \mathrm{BL}}{\mathrm{BL}} = \gamma^2 |g^{(1)}(\tau)|^2 \qquad (1)$$

where t is time, τ means correlation delay time,

$$G^{(2)}(\tau) = \int_{-\infty}^{\infty} I(t)\, I(t+\tau)\, \mathrm{d}t \qquad (2)$$

is the time autocorrelation function of the scattered-radiation intensity I measured by a detector,[3]

$$\mathrm{BL} = \left(\int_{-\infty}^{\infty} \mathbf{E}^*(t)\, \mathbf{E}(t)\, \mathrm{d}t\right)^2 \qquad (3)$$

is the baseline of the intensity ACF, $\mathbf{E}$ denotes the vector of electric field which contains both single-scattering and multiple−scattering contributions, $|g^{(1)}(\tau)|$ is the measured normalized field autocorrelation function, and the coherence factor γ depends on the method of detection being used.[1,4−7]

For the most practical cases when the hydrodynamic interaction of particles does not affect sufficiently Gaussian

* Author to whom correspondence should be addressed. E-mail: vovod@worldnet.att.net.

(1) Brown, W. Dynamic Light Scattering. The Method and Some Applications; Clarendon Press: Oxford, 1993.

(2) Finsy, R. Particle Sizing by Quasi-Elastic Light Scattering. *Adv. Colloid Interface Sci.* **1994**, *52*, 79−143.

(3) Lock, J. A. The Role of Multiple Scattering in Cross-Correlated Light Scattering Employing a Single Laser Beam. *Appl. Opt.* **1997**, *36*, 7559−7570.

(4) Dhadwal, H. S.; Wu, W.; Chu, B. A Fiber-Optic Light-Scattering *Spectrometer. Rev. Sci. Instrum.* **1989**, *60*, 845−853.

(5) Suparno; Deurloo, K.; Stamatelopolous, P.; Srivastva, R.; Thomas, J. C. Light Scattering with Single-Mode Fiber Collimators. *Appl. Opt.* **1994**, *33*, 7200−7205.

(6) Ricka, J. Dynamic Light Scattering with Single-Mode and Multimode Receivers. *Appl. Opt.* **1993**, *32*, 2860−2875.

(7) Gisler, T.; Rüger, H.; Egelhaaf, S. U.; Tschumi, J.; Schurtenberger, P.; Ricka, J. Mode-Selective Dynamic Light Scattering: Theory Versus Experimental Realization. *Appl. Opt.* **1995**, *34*, 3546−3353.

S0743-7463(96)02130-0 CCC: $15.00
Published on Web 04/15/1998

stochastics of the scattered electric field, one can use Wick's theorem[3,8] to expand eq 2 in products of the electric field:

$$G^{(2)}(\tau) \approx \mathrm{BL} + |Y|^2 + |W|^2 \tag{4}$$

where

$$Y = \int_{-\infty}^{\infty} \mathbf{E}(t)\, \mathbf{E}(t+\tau)\, \mathrm{d}t,$$
$$W = \int_{-\infty}^{\infty} \mathbf{E}^*(t)\, \mathbf{E}(t+\tau)\, \mathrm{d}t \tag{5}$$

A. Particle Sizing in Diluted Suspensions. In a diluted suspension, particle dynamics can be described by Brownian motion of noninteracting (free) particles. The Brownian motion of monodispersed particles is characterized by the Stokes–Einstein free-diffusion coefficient D_0 and/or the mean-squared displacement of a free particle after a time t[9]

$$\langle |\Delta \mathbf{X}(t, \varphi \to 0)|^2 \rangle = 6 D_0 t \tag{6}$$

where φ is the volume fraction of the solid and $\langle ... \rangle$ denotes ensemble averaging.

Particle size measurements in highly diluted dispersions are easy because the multiple scattering by particles and their interactions are negligible. In this case when $\varphi \to 0$, the field ACF has a simple exponential behavior:[1-7]

$$|g_0^{(1)}(\tau)| = |g^{(1)}(\tau, \varphi \to 0)| = \exp\left(-\frac{\tau}{\tau^*}\right) \tag{7}$$

We assume the far field location of a detector when the scattered vector of each ith particle, $\mathbf{k}_s^i$, coincides with the scattered vector of the measurement volume, $\mathbf{k}_s$, that is,

$$\mathbf{k}_s^i \approx \mathbf{k}_s \tag{8}$$

where the scattered vectors defined as

$$\mathbf{k}_s^i = \frac{\bar{\bar{k}}_0 \mathbf{R}_d^i}{R_d^i}, \quad \mathbf{k}_s = \frac{\bar{\bar{k}}_0 \mathbf{R}_d}{R_d} \tag{9}$$

$\bar{\bar{k}}_0$ is the wavenumber of the light in the liquid, $\mathbf{R}_d^i$ and $\mathbf{R}_d$ are the position vectors of a detector relative origins of the ith particle in the ensemble and the particle ensemble, respectively. In the far field assumption, the infinite-dilution self-diffusion coefficient D_0 of monodispersed free particles and their hydrodynamic diameter d_p can be deduced from the measured ACF decay time τ^*

$$D_0 = \frac{1}{\tau^* q^2} \tag{10}$$

$$d_p = \frac{k_B T}{3\eta} \tau^* q^2 \tag{11}$$

where k_B is Boltzmann's constant, T is the absolute temperature, η is the viscosity of the suspending medium, q is the magnitude of the scattering wave vector $\mathbf{q}$ of the entire particle-ensemble,

$$q = |\mathbf{q}| = |\mathbf{k}_0 - \mathbf{k}_s| \tag{12}$$

$\mathbf{k}_0$ is the incident wave vector.

In this paper, we outline the case of polydispersed particles (the size distribution of Brownian particles can be recovered by employing variety techniques[1,10-12]) and focus on measurement problems in turbid media.

B. Measurement Problems in Concentrated Dispersions. General problems of particle sizing in turbid media (when $\varphi > 0$) by PCS are dynamics of interacting particles and multiple scattering of light by particles. Interaction of particles contributes to the deviation of the relative mean-squared displacement from the unit[9]

$$\mathrm{RMSD}(\tau, \varphi) = \frac{\langle |\Delta \mathbf{X}(\tau, \varphi)|^2 \rangle}{\langle |\Delta \mathbf{X}(\tau, \varphi \to 0)|^2 \rangle} \le 1 \tag{13}$$

Both the particle interactions and multiple scattering affect an exponential behavior of ACF shown by eq 7. This affect can be described numerically by the relative diffusion coefficient (RDC)

$$\mathrm{RDC}(\tau, \varphi) = \frac{\mathrm{D}(\tau, \varphi)}{D_0} = \frac{\ln(|g^{(1)}(\tau, \varphi)|)}{\ln(|g_0^{(1)}(\tau)|)} = \frac{\ln(|g^{(1)}(\tau, \varphi)|)}{\tau/\tau^*} \tag{14}$$

and/or by the relative mean-diffusion coefficient (RMDC)

$$\mathrm{RMDC}(\tau_d, \varphi) = \frac{\langle D(\tau_d, \varphi) \rangle}{D_0} = \frac{\langle \ln(|g^{(1)}(\tau_d, \varphi)|) \rangle}{\tau/\tau^*} \tag{15}$$

where $\tau_d \le \tau_{max}$ is the dynamic delay-time range of ACF over which the last average is provided, $D(\tau,\varphi)$ is the diffusion coefficient corresponding to the τ delay time of the ACF, and τ_{max} is the upper range of the investigated delay time.

Main experimental[13-17] and theoretical[17-23] efforts in particle sizing of turbid media by PCS are focused on the

(8) Dhont, J. K. G.; de Kruif, C. G. Scattered Light Intensity Cross Correlation. 1. Theory. *J. Chem. Phys.* **1983**, *79*, 1658–1663.

(9) Hockney, R. W.; Eastwood, J. W. *Computer Simulation Using Particles*; Institute of Physics Publishing: Bristol and Philadelphia, 1988; p 485.

(10) Stramski, D.; Sedlak, M. Application of Dynamic Light Scattering to Study of Small Marine Particles. *Appl. Opt.* **1994**, *33*, 4825–4834.

(11) Beretta, S.; Lunelli, L.; Chirico, G.; Baldini, G. Dynamic Light Scattering from Small Particles: Expected Accuracy in Hemoglobin Data Reduction. *Appl. Opt.* **1996**, *35*, 3763–3770.

(12) Brenci, M.; Mencaglia, A.; Mignani, A. G.; Pieraccini, M. Circular-Array Optical-Fiber Probe for Backscattering Photon Correlation Spectroscopy Measurements. *Appl. Opt.* **1996**, *35*, 6775–6780.

(13) Horne, D. S. Particle Size Measurement in Concentrated Latex Suspensions Using Fiber-Optic Photon Correlation Spectroscopy. *J. Phys. D: Appl. Phys.* **1989**, *22*, 1257–1265.

(14) Wiese, H.; Horn, D. Single-Mode Fibers in Fiber-Optic Quasielastic Light Scattering: A Study of the Dynamics of Concentrated Latex Dispersions. *J. Chem. Phys.* **1991**, *94*, 6429–6443.

(15) Dhadwal, H. S.; Ansar, R. R.; Meyer, W. V. A Fiber-Optic Probe for Particle Sizing in Concentrated Suspensions. *Rev. Sci. Instrum.* **1991**, *62*, 2963–2968.

(16) Meyer, W. V.; Cannel, D. S.; Taylor, T. W.; Tin, P.; Smart, A. E.; Zhu, J.; Cheung, H. M.; Mann, J. A. A Single Wavelength Cross-Correlation Technique Which Suppresses Multiple Scattering. In Proceedings of the Photon Correlation & Scattering, Capri, Italy, Aug 1996; 1996; pp 104–107.

(17) Xue, J.-Z.; Wu, X.-L.; Pine, D. J.; Chaikin, P. M. Hydrodynamic Interactions in Hard-Sphere Suspensions. *Phys. Rev.* **1992**, *45*, 989–993.

(18) Hoekstra, A. G.; Sloot, P. M. A. Coupled Dipole Simulations of Elastic Light Scattering on Parallel Systems. *Int. J. Mod. Phys. C* **1995**, *6*, 663–679.

(19) Shanks, J. G.; Sengers, J. V. Double Scattering in Critically Opalescent Fluids. *Phys. Rev. A* **1988**, *38*, 885–896.

(20) Sorenson, C. M.; Mockler, R. C.; O'Sullivan, W. J. Depolarized Correlation Functions of Light Double Scattered from a System of Brownian Particles. *Phys. Rev. A* **1976**, *14*, 1520–1532.

stochastics of the scattered electric field, one can use Wick's theorem[3,8] to expand eq 2 in products of the electric field:

$$G^{(2)}(\tau) \approx \mathrm{BL} + |Y|^2 + |W|^2 \tag{4}$$

where

$$Y = \int_{-\infty}^{\infty} \mathbf{E}(t)\, \mathbf{E}(t+\tau)\, \mathrm{d}t,$$
$$W = \int_{-\infty}^{\infty} \mathbf{E}^*(t)\, \mathbf{E}(t+\tau)\, \mathrm{d}t \tag{5}$$

A. Particle Sizing in Diluted Suspensions. In a diluted suspension, particle dynamics can be described by Brownian motion of noninteracting (free) particles. The Brownian motion of monodispersed particles is characterized by the Stokes–Einstein free-diffusion coefficient D_0 and/or the mean-squared displacement of a free particle after a time t[9]

$$\langle |\Delta \mathbf{X}(t, \varphi \to 0)|^2 \rangle = 6 D_0 t \tag{6}$$

where φ is the volume fraction of the solid and $\langle ... \rangle$ denotes ensemble averaging.

Particle size measurements in highly diluted dispersions are easy because the multiple scattering by particles and their interactions are negligible. In this case when $\varphi \to 0$, the field ACF has a simple exponential behavior:[1-7]

$$|g_0^{(1)}(\tau)| = |g^{(1)}(\tau, \varphi \to 0)| = \exp\left(-\frac{\tau}{\tau^*}\right) \tag{7}$$

We assume the far field location of a detector when the scattered vector of each ith particle, $\mathbf{k}_s^i$, coincides with the scattered vector of the measurement volume, $\mathbf{k}_s$, that is,

$$\mathbf{k}_s^i \approx \mathbf{k}_s \tag{8}$$

where the scattered vectors defined as

$$\mathbf{k}_s^i = \frac{\bar{\bar{k}}_0 \mathbf{R}_d^i}{R_d^i}, \quad \mathbf{k}_s = \frac{\bar{\bar{k}}_0 \mathbf{R}_d}{R_d} \tag{9}$$

$\bar{\bar{k}}_0$ is the wavenumber of the light in the liquid, $\mathbf{R}_d^i$ and $\mathbf{R}_d$ are the position vectors of a detector relative origins of the ith particle in the ensemble and the particle ensemble, respectively. In the far field assumption, the infinite-dilution self-diffusion coefficient D_0 of monodispersed free particles and their hydrodynamic diameter d_p can be deduced from the measured ACF decay time τ^*

$$D_0 = \frac{1}{\tau^* q^2} \tag{10}$$

$$d_p = \frac{k_B T}{3\eta} \tau^* q^2 \tag{11}$$

where k_B is Boltzmann's constant, T is the absolute temperature, η is the viscosity of the suspending medium, q is the magnitude of the scattering wave vector $\mathbf{q}$ of the entire particle-ensemble,

$$q = |\mathbf{q}| = |\mathbf{k}_0 - \mathbf{k}_s| \tag{12}$$

$\mathbf{k}_0$ is the incident wave vector.

In this paper, we outline the case of polydispersed particles (the size distribution of Brownian particles can be recovered by employing variety techniques[1,10-12]) and focus on measurement problems in turbid media.

B. Measurement Problems in Concentrated Dispersions. General problems of particle sizing in turbid media (when $\varphi > 0$) by PCS are dynamics of interacting particles and multiple scattering of light by particles. Interaction of particles contributes to the deviation of the relative mean-squared displacement from the unit[9]

$$\mathrm{RMSD}(\tau, \varphi) = \frac{\langle |\Delta \mathbf{X}(\tau, \varphi)|^2 \rangle}{\langle |\Delta \mathbf{X}(\tau, \varphi \to 0)|^2 \rangle} \le 1 \tag{13}$$

Both the particle interactions and multiple scattering affect an exponential behavior of ACF shown by eq 7. This affect can be described numerically by the relative diffusion coefficient (RDC)

$$\mathrm{RDC}(\tau, \varphi) = \frac{\mathrm{D}(\tau, \varphi)}{D_0} = \frac{\ln(|g^{(1)}(\tau, \varphi)|)}{\ln(|g_0^{(1)}(\tau)|)} = -\frac{\ln(|g^{(1)}(\tau, \varphi)|)}{\tau/\tau^*} \tag{14}$$

and/or by the relative mean-diffusion coefficient (RMDC)

$$\mathrm{RMDC}(\tau_d, \varphi) = \frac{\langle D(\tau_d, \varphi) \rangle}{D_0} = -\frac{\langle \ln(|g^{(1)}(\tau_d, \varphi)|) \rangle}{\tau/\tau^*} \tag{15}$$

where $\tau_d \le \tau_{max}$ is the dynamic delay-time range of ACF over which the last average is provided, $D(\tau,\varphi)$ is the diffusion coefficient corresponding to the τ delay time of the ACF, and τ_{max} is the upper range of the investigated delay time.

Main experimental[13-17] and theoretical[17-23] efforts in particle sizing of turbid media by PCS are focused on the

(8) Dhont, J. K. G.; de Kruif, C. G. Scattered Light Intensity Cross Correlation. 1. Theory. *J. Chem. Phys.* **1983**, *79*, 1658–1663.
(9) Hockney, R. W.; Eastwood, J. W. *Computer Simulation Using Particles*; Institute of Physics Publishing: Bristol and Philadelphia, 1988; p 485.
(10) Stramski, D.; Sedlak, M. Application of Dynamic Light Scattering to Study of Small Marine Particles. *Appl. Opt.* **1994**, *33*, 4825–4834.
(11) Beretta, S.; Lunelli, L.; Chirico, G.; Baldini, G. Dynamic Light Scattering from Small Particles: Expected Accuracy in Hemoglobin Data Reduction. *Appl. Opt.* **1996**, *35*, 3763–3770.
(12) Brenci, M.; Mencaglia, A.; Mignani, A. G.; Pieraccini, M. Circular-Array Optical-Fiber Probe for Backscattering Photon Correlation Spectroscopy Measurements. *Appl. Opt.* **1996**, *35*, 6775–6780.
(13) Horne, D. S. Particle Size Measurement in Concentrated Latex Suspensions Using Fiber-Optic Photon Correlation Spectroscopy. *J. Phys. D: Appl. Phys.* **1989**, *22*, 1257–1265.
(14) Wiese, H.; Horn, D. Single-Mode Fibers in Fiber-Optic Quasielastic Light Scattering: A Study of the Dynamics of Concentrated Latex Dispersions. *J. Chem. Phys.* **1991**, *94*, 6429–6443.
(15) Dhadwal, H. S.; Ansar, R. R.; Meyer, W. V. A Fiber-Optic Probe for Particle Sizing in Concentrated Suspensions. *Rev. Sci. Instrum.* **1991**, *62*, 2963–2968.
(16) Meyer, W. V.; Cannel, D. S.; Taylor, T. W.; Tin, P.; Smart, A. E.; Zhu, J.; Cheung, H. M.; Mann, J. A. A Single Wavelength Cross-Correlation Technique Which Suppresses Multiple Scattering. In Proceedings of the Photon Correlation & Scattering, Capri, Italy, Aug 1996; 1996; pp 104–107.
(17) Xue, J.-Z.; Wu, X.-L.; Pine, D. J.; Chaikin, P. M. Hydrodynamic Interactions in Hard-Sphere Suspensions. *Phys. Rev.* **1992**, *45*, 989–993.
(18) Hoekstra, A. G.; Sloot, P. M. A. Coupled Dipole Simulations of Elastic Light Scattering on Parallel Systems. *Int. J. Mod. Phys. C* **1995**, *6*, 663–679.
(19) Shanks, J. G.; Sengers, J. V. Double Scattering in Critically Opalescent Fluids. *Phys. Rev. A* **1988**, *38*, 885–896.
(20) Sorenson, C. M.; Mockler, R. C.; O'Sullivan, W. J. Depolarized Correlation Functions of Light Double Scattered from a System of Brownian Particles. *Phys. Rev. A* **1976**, *14*, 1520–1532.

investigation and explanation of the ACF distortion by particles interaction and multiple scattering.

In this paper, we introduce a technique[24] for numerical modeling of the effects of particle dynamics and multiple scattering on the first-order ACF, $|g^{(1)}(\varphi, \tau)|$, of the electric field scattered from a concentrated dispersion illuminated by a plane wave. We use the following expression to model the first-order ACF:

$$g^{(1)}(\tau, \varphi) = \frac{\int_0^{t_{max}} \mathbf{E}(t+\tau)\,\mathbf{E}^*(t)\,dt}{\int_0^{t_{max}} \mathbf{E}(t)\,\mathbf{E}^*(t)\,dt} \tag{16}$$

which can be derived from eqs 1−5 when the $|Y|^2$ term is neglected with respect to $|W|^2$ in eq 4, as it has done in ref 3. The technique is based on the fast numerical integration eq 16 over the upper time range, t_{max}, required for a given calculation accuracy, and on the rigorous simulation[25,26] (instead of an approximation[1,19−22,27]) of the vector $\mathbf{E}(t)$ of the scattered electric field. We show that the proposed model can be used effectively for the separate investigations of dynamics and multiple-scattering effects in PCS. Comprehensive modeling of the intensity ACF, including coherence factor γ and the baseline BL, is provided in another paper[28] taking into account the $|Y|^2$ term.

2. Overview of the Model

A. Considerations. The following considerations are taken into account in the proposed model: (1) an ensemble of N_p hard spheres randomly packed inside a cubic volume is used as a model of a concentrated dispersion[25−27] at a given time t; (2) spheres are monodispersed; (3) plane wave is incident upon an ensemble instead of a real light beam; (4) the plane wave is assumed to be polarized in the x-direction; (5) the field-scattered electric from the ensemble is detected inside the unit solid angle $d\Omega_s = \sin\theta_s\, d\varphi_s\, d\theta_s$ of the scattered vector $\mathbf{k}_s$ (where θ_s and φ_s are the angle coordinates of the cathode center of a detector in the spherical coordinate system of the ensemble origin).

A flow diagram to model measurements in PCS is presented in Figure 1.

B. Input Data. The input data involve the diameter d_p of monodispersed particles, volume fraction φ of a solid in dispersion, refractive index m_p of particles, refractive index n_m of the solvent of a dispersed media, wave vector $\mathbf{k}_0$ of the incident plane wave, scattered vector $\mathbf{k}_s$, relation τ_{max}/τ^* specifying the upper range of the investigated delay time, and the allowable value of the calculation error ϵ.

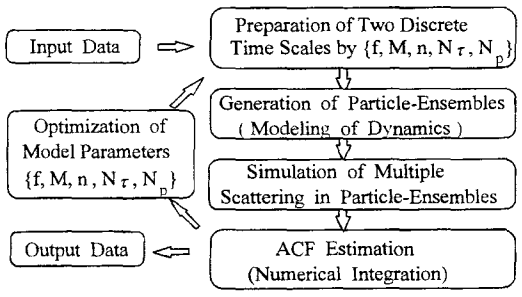

Figure 1. Flow diagram of simulations.

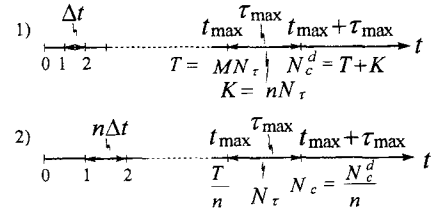

Figure 2. Two discrete scales of time: (1) time scale for particle-dynamics generation; (2) time scale for the multiple-scattering simulation and the ACF estimation by numerical integration in eq 16.

C. Preparation of Two Discrete Time Scales. In the initial stage of calculation, a set of nondimensional model parameters $\{f, M, n, N_\tau\}$ are generated for the preparation of two discrete time scales as shown in Figure 2.

The first scale of time with the time step Δt is prepared for generation of particle dynamics. The second scale with the time step $n\Delta t$ is for the simulation of multiple scattering and for numerical integration in eq 16. The integer coefficient n is employed for decreasing the number of integration intervals. One chooses the number N_τ of points in the second (integration) time scale for the presentation of ACF modeled on the delay-time range τ_{max} given by

$$\tau_{max} = K\Delta t \tag{17}$$

where

$$K = nN_\tau \tag{18}$$

is the upper range of the relative delay time in the dynamics time scale. Integer M (and/or T, see Figure 2) specifies the upper time range t_{max} of integration

$$T = \frac{t_{max}}{\Delta t} = MN_\tau \tag{19}$$

The parameter f prescribes the mean-squared displacement of free particles after a short unit time step Δt by

$$\langle|\Delta\mathbf{X}(\Delta\tau, \varphi \to 0)|^2\rangle = \left(\frac{f}{q}\right)^2 \tag{20}$$

where

$$q = 2k_0 \sin\frac{\theta_s}{2} \tag{21}$$

follows form eq 12 and

$$k_0 = \frac{2\pi}{\lambda} n_m \tag{22}$$

(21) Dhont, J. K. G. Multiple Rayleich-Gans-Debye Scattereing in Colloidal Systems-Dynamic Light Scattering. *Physica* **1985**, *129A*, 374−394.

(22) Dhont, J. K. G. Light Scattering from Colloidal Systems in the Rayleich-Gans-Debye Approximation. Ph.D. Thesis, Rijks Universiteit te Utrecht, The Netherlands, 1985; p 107.

(23) Bailey, A. E.; Cannell, D. S. Practical Method for Calculation of Multiple Light-Scattering. *Phys. Rev. E* **1994**, *50*, 4853−4864.

(24) Ovod, V. I. Characterization of Particles and Particulate Polluants in Concentrated and Turbid Media by Photon Correlation Spectroscopy. Scientific report; Department of Theoretical Physical Chemistry, Vrije Universiteit Brussel: Brussels, Belguim, Aug 1996; pp 81−108.

(25) Borghese, F.; Denti, P.; Toscano, G.; Sindoni, O. I. Electromagnetic Scattering by a Cluster of Spheres. *Appl. Opt.* **1979**, *18*, 116−120.

(26) Mackowski, D. W. Calculation of Total Cross Sections of Multiple-Sphere Clusters. *J. Opt. Soc. Am. A* **1994**, *11*, 2851−2861.

(27) Markel, V. A.; Shalaev, V. M.; Poliakov, E. Y. Fluctuations of Light Scattered by Fractal Clusters. *J. Opt. Soc. Am. A* **1997**, *14*, 60−69.

(28) Ovod, V. I. Modeling of Multiple Scattering Suppression in Photon Correlation Spectroscopy. In *Proceedings of the Third Workshop on Electromagnetic and Light Scattering—Theory and Applications* (University of Bremen) March 1988; pp 239−248.

Table 1. Many-Body Hydrodynamic Factor for the High-q Limit vs the Volume Fraction φ of Solid[a]

φ	0	0.05	0.1	0.15	0.2	0.25	0.3	0.35	0.4	0.45
$H(q \to 0,\varphi)$	1	0.9	0.79	0.69	0.6	0.51	0.44	0.38	0.33	0.28

[a] Data are borrowed from ref 30 (p 362).

is the wavenumber of the incident radiation in the solvent of the dispersed media.

Taking into account eqs 6, 10, 17, 18, and 20, one can derive the following equations for the decay time τ^*, the relative upper delay time range τ_{max}/τ^* of the modeled ACF, and the unit time step in the proposed discrete time scales, respectively: and

$$\tau^* = \frac{6}{f^2}\Delta t \tag{23}$$

$$\frac{\tau_{max}}{\tau^*} = \frac{nN_\tau f^2}{6} \tag{24}$$

$$\Delta t = \left(\frac{f}{q}\right)^2 \frac{1}{6D_0} \tag{25}$$

D. Modeling of Particle Dynamics. *Dynamics of Interacting Particles.* In the second stage of simulation, the dynamics of interacting particles is modeled by using the algorithm of randomly close-packed hard spheres (CPHS).[27] According to this algorithm, a time set of N_c^d particle-ensembles is generated in order to model the motion of particles over the time range $t_{max} + \tau_{max}$. The number of generated particle-ensembles is given by

$$N_c^d = \frac{t_{max} + \tau_{max}}{\Delta t} = T + K \tag{26}$$

and the length of the cubic ensemble can be found from

$$l_c = d_p\left(\frac{\pi N_p}{6\varphi}\right)^{1/3} \tag{27}$$

The initial position vector $\mathbf{X}(c = 1, i)$ of each ith particle and a new position $\mathbf{X}(c, i)$ after the cth step of motion are chosen randomly inside the cth ensemble (the space condition). Motion of any ith particle is described by its position vector in the Cartesian xyz-coordinate system of cth ensemble by

$$\mathbf{X}(c, i) = \mathbf{X}(c - 1, i) + \mathbf{s}|\Delta\mathbf{X}(\varphi)| \qquad \text{for } j \geq 2 \tag{28}$$

where

$$\mathbf{s} = s_x\mathbf{x} + s_y\mathbf{y} + s_z\mathbf{z} \tag{29}$$

is the unit random vector. At each cth step, the space and intersection conditions are checked: if the newly placed ith sphere is outside of the cth ensemble and/or if the distance between the origin of this sphere and the origin of any previously placed sphere is less than the sum of their radii, this cth step of the ith sphere is rejected and the next random position is tried.

To generate the unit random vector $\mathbf{s}$, the function ran2-(*idum*) is taken from ref 29. This function is recommended (ref 29, pp 272, 276) for generating more than 100 000 000 random numbers in a single calculation. The parameter *idum* (defined in ref 29) is used for initialization of the generator. A new magnitude of this parameter is responsible for a new history of generated particle ensembles.

To decrease the upper time range t_{max} of the integration in eq 16, the squared magnitude of the modeled unit displacement $|\Delta\mathbf{X}(\varphi)|^2$ is equal to the mean-squared displacement $\langle|\Delta\mathbf{X}(\varphi)|^2\rangle$ characterizing the real motion of particles after the discrete time Δt,[9] that is,

$$|\Delta\mathbf{X}(\varphi)| = \sqrt{\langle|\Delta\mathbf{X}(\varphi)|^2\rangle} \tag{30}$$

To take into account the effect of many-body hydrodynamic interaction, the short-time self-diffusion coefficient $D_s^{(st)}(\varphi)$, comprehensively investigated by C. W. J. Beenakker and P. Mazur,[30] is employed for estimation of the real mean-squared particle displacement after a short discrete time Δt:

$$\langle|\Delta\mathbf{X}(\varphi)|^2\rangle = D_s^{(st)}(\varphi)6\Delta t \tag{31}$$

As follows from the analysis of eqs 20, 30, and 31, the influence of the hydrodynamic interactions on the modeled unit displacement can be described by

$$|\Delta\mathbf{X}(\varphi)| = \sqrt{H(q \to \infty, \varphi)}\,\frac{f}{q} \tag{32}$$

where

$$H(q \to \infty, \varphi) = \frac{D_s^{(st)}(\tau \to 0, \varphi)}{D_0} \tag{33}$$

is the hydrodynamic interaction factor for the high-q limit defined in refs 17, 30, and 31. For our simulations, we borrow the many-body hydrodynamic factor from ref 30. This factor is presented in Table 1.

Parameter f should be chosen taking into account the criterion

$$f \ll qd_p\sqrt{\frac{\pi}{6\varphi}}\,\frac{1}{H(q \to \infty, \varphi)} \tag{34}$$

which follows from the requirement for any numerical model for turbid dispersions (ref 31, p 5826), that is,

$$|\Delta\mathbf{X}(\varphi)| \ll \sqrt{\langle|\Delta r(\varphi)|^2\rangle} \tag{35}$$

where

$$\sqrt{\langle|\Delta r(\varphi)|^2\rangle} = d_p\sqrt{\frac{\pi}{6\varphi}} \tag{36}$$

is the mean interparticle spacing.

Brownian Motion. If Brownian motion ($\varphi \to 0$) is generated, neither the intersection condition mentioned above nor the space condition is checked.

E. Multiple-Scattering Simulations. In the next stage of modeling (see Figure 1), a new set of N_c particle-

(29) Press, W. H.; Teukolsky, S. A.; Vetterling, W. T.; Flannery, B. P. *Numerical Recipes in FORTRAN. The Art of Scientific Computing.* Cambridge University Press: Cambridge, U.K., 1994.

(30) Beenakker, C. W. J.; Mazur, P. Diffusion of Spheres in a Concentrated Suspension II. *Physica* **1984**, *126A*, 349–370.

(31) Snook, I.; van Megen, W. Diffusion in Concentrated Hard Sphere Dispersions: Effective Two Particle Mobility Tensors. *J. Chem. Phys.* **1983**, *78*, 5825–5836.

ensembles is prepared for the simulation of multiple scattering and for ACF simulation, that is,

$$N_c = \frac{N_c^d}{n} \tag{37}$$

This new set involves each nth ensemble from the original set of N_c^d particle-ensembles (see Figure 2). The vector $\mathbf{E}(c)$ of the electric field scattered by each cth ensemble from the new set of particle-ensembles is calculated by using a rigorous algorithm based on the superposition solution: the scattered electric field from the entire cth ensemble $\mathbf{E}(c)$ is taken to be the superposition of scattered fields E^i from each of the spheres in the ensemble,[25,26] that is:

$$\mathbf{E}(c) = \sum_i^{N_p} \mathbf{E}^i \tag{38}$$

We employ D. W. Mackowski's fast technique to simulate the combined scattered field $\mathbf{E}(c)$ from all spheres by using the a_{mn}^c and b_{mn}^c single-expansion coefficients of multiple scattering, written about the origin of the cth ensemble:[26]

$$\mathbf{E}(c) = \sum_{l=1}^{l_{max}} \sum_{m=-l}^{l} [a_{lm}^c \mathbf{N}_{lm}^{(3)}(k_i \mathbf{R}_d) + b_{lm}^c \mathbf{M}_{lm}^{(3)}(k_i \mathbf{R}_d)] \tag{39}$$

where $\mathbf{N}^{(3)}$ and $\mathbf{M}^{(3)}$ are vector harmonics,[32] the subscript l is the partial wavenumber, m is the muthal mode number,

$$l_{max} \approx \max\{r^{ij} + 4(r^{ij})^{1/3} + 2\} \tag{40}$$

is the required partial wavenumber,

$$r^{ij} = \rho + X^{ij} \tag{41}$$

X^{ij} is the distance between the ith and jth particle, and

$$\rho = \frac{\pi d_p}{\lambda} n_m \tag{42}$$

is the Mie parameter of a particle. Calculation of the additional, scattered-field, and incident-field expansion coefficients is discussed in refs 26 and 33.

F. ACF Simulation. *Multiple-Scattering Scheme for ACF Simulation.* To decrease the upper time range t_{max} of integration in eq 16 required for a given ACF calculation error, an additional average over the number N_q of different scattering vectors $\mathbf{q}$ having the same magnitudes is employed, i.e.,

$$g^{(1)}(\tau, \varphi) = \frac{1}{\mathbf{N_q}} \sum_{q=1}^{\mathbf{N_q}} \frac{\int_0^{t_{max}} \mathbf{E}(t+\tau)\, \mathbf{E}^*(t)\, dt}{\int_0^{t_{max}} \mathbf{E}(t)\, \mathbf{E}^*(t)\, dt} \tag{43}$$

Integrals are calculated by using the trapezoidal rule (ref 29, p 127):

$$g^{(1)}(\tau, \varphi) = \frac{1}{N_q} \sum_{q=1}^{N_q} \frac{\sum_{l=1}^{T/n} \mathbf{E}(c+k)\, \mathbf{E}^*(c)}{\sum_{l=1}^{T/n} \mathbf{E}(c)\, \mathbf{E}^*(c)} \tag{44}$$

where the scattered electric field is simulated by eq 39 and

$$k = \frac{\tau}{\Delta t}, \qquad c = \frac{t}{\Delta t} \tag{45}$$

are the discrete relative delay time and the relative time (current number of a particle-ensemble), respectively. As D. W. Mackowski has shown in ref 26, averaging over the scattering vectors $\mathbf{q}$ economizes also the computation time, because matrices of the addition A and B coefficients defined in ref 26 are simulated once for each cth ensemble and are used for any direction of the plane wave.

Structure-Factors Approach. Structure-factors (ref 1, p 325)[14] approach is employed often instead of rigorous numerical simulations for explaining the effects of particle interaction on experimental data in PCS. These approaches can be derived from eq 44 for the far field detection of scattered light if only phase factors of the electric field are taken into account:

$$g^{(1)}(\tau, \varphi) = \frac{F(\tau, \varphi)}{S(\varphi)} \tag{46}$$

where

$$F(\tau, \varphi) = \frac{1}{\mathbf{N_q}\left(\frac{T}{n} - 1\right) N_p} \times \sum_{u=1}^{N_q} \sum_{l=1}^{T/n} \sum_{i=1}^{N_p} \sum_{j=1, j\neq i}^{N_p} \exp[i\mathbf{q}_u(\mathbf{X}^i(c+k) - \mathbf{X}^j(k))] \tag{47}$$

is the dynamic structure factor

$$S(\varphi) = F(\tau \to 0, \varphi) \tag{48}$$

is the static structure factor, and i is the imaginary unit. If $j \neq i$, eq 47 gives the so-called normalized coherent or full-dynamic structure factor $F(\tau, \varphi)$.[14] Otherwise, the cross terms are omitted, and the normalized self-dynamic structure factor $F_s(\tau, \varphi)$ is simulated.

In our model, only three fixed orientations of the scattered vector $\mathbf{q}$ are used – along the x-, y-, and z-axes of the ensemble's coordinate system. These orientations permit the simplification of eq 47 by

$$F(\tau, \varphi) = \frac{1}{3\left(\frac{T}{n} - 1\right) N_p} \times \sum_{h=x,y,z} \sum_{l=1}^{T/n} \sum_{i=1}^{N_p} \sum_{j=1, j\neq i}^{N_p} \exp[iqh(i, j, c+k)] \tag{49}$$

where

$$h(i, j, c, k) = h^i(c+k) - h^j(k) \tag{50}$$

$h^i(c+k)$ denotes x-, y-, or z-coordinates of the ith particle in the $(c+k)$ ensemble.

(32) Bohren, C. F.; Haffman, D. R. *Absorption and Scattering of Light by Small Particles*; Wiley: New York, 1983.
(33) Mackowski, D. W. Analysis of Radiative Scattering for Multiple Sphere Configurations. *Proc. R. Soc. London A* **1991**, *433*, 599–614.
(34) Allen, M. P.; Tildesley, D. J. Computer Simulation of Liquids. The Ipswich Book Co Ltd, 1993.

G. Output Data. The output data are the modeled relative mean-squared displacement of particles eq 13, ACF, and the relative mean-diffusion coefficient eq 15. Output data, obtained for the same history of the modeled particle dynamics by using the rigorous multiple-scattering simulation (eq 44), full and self-dynamic factors (eqs 47 or 49), permit the separation of the effects of multiple scattering and particle dynamics on measurement results in PCS.

3. Model Optimization

The majority of calculation expenditures, or run times, are related to the calculations of multiple scattering from an ensemble. These expenditures strongly depend on the number of particles N_p in an ensemble and on the number of particle-ensembles N_c.[26] Thus, to model PCS measurements in a reasonable length of time, the number of particles and the number of particle-ensembles N_c are to be minimized. This minimization however can lead to numerical errors in the modeling of particle dynamics and ACF. The goal of model optimization is to search for a compromise between the computation time and numerical accuracy of the modeling.

A. Errors of the Numerical Model. Numerical errors of the model can be estimated in the regime of free-particle diffusion ($\varphi \to 0$) when the effect of multiple scattering is negligible: in this regime, all distortion of ACF is caused by calculation errors of the model. The error of the modeled Brownian particle dynamics is defined by

$$\epsilon_d(\tau) = \mathrm{RMSD}(\tau, \varphi \to 0) - 1 \tag{51}$$

The systematic error of the ACF modeling is given by

$$\epsilon_a(\tau) = \mathrm{RDC}(\tau, \varphi \to 0) - 1 \tag{52}$$

and the model error averaged over the dynamic range τ_d is specified by

$$\langle \epsilon_a(\tau_d) \rangle = \mathrm{RMDC}(\tau_d, \varphi \to 0) - 1 \tag{53}$$

where the relative mean-squared displacement (RMSD), the relative diffusion coefficient (RDC), and the relative mean-diffusion coefficient (RMDC) are defined by eqs 13–15, respectively.

On the stage of the optimization when only Brownian motion is modeled, and when the rigorous eq 44 and the self-diffusion approach ($i = j$) give similar results, that is,

$$g^{(1)}(\tau, \varphi \to 0) \approx F_s(\tau, \varphi \to 0) \tag{54}$$

we recommend economizing the calculation time by using the self-diffusion approach, eq 49, rather than the rigorous eq 44.

B. Optimization Criteria of the Numerical Model. Simulations indicate that the errors with ACF modeling are larger than those with dynamics because of an additional error in numerical integration by eq 44 or 49, that is,

$$|\epsilon_a(\tau)| \gg |\epsilon_d(\tau)| \tag{55}$$

and even

$$\left| \left\langle \epsilon_a\left(\frac{\tau_d}{\tau^*}\right) \right\rangle \right| \gg |\epsilon_d(\tau)| \tag{56}$$

Taking the above-mentioned into account, the following criteria can be used for optimization of the main model parameters set $\{f, M, n, N_r\}$:

$$\min\left\{N_c, N_p, \left|\epsilon_a\left(\frac{\tau_r}{\tau^*}\right)\right|, \frac{\tau^*}{\tau_{dm}}\right\} \tag{57}$$

and/or

$$\min\left\{N_c, N_p, \left|\left\langle \epsilon_a\left(\frac{\tau_{dm}}{\tau^*}\right)\right\rangle\right|, \frac{\tau^*}{\tau_{dm}}\right\} \tag{58}$$

where τ_r/τ^* is the relative reference delay time chosen for estimation of numerical accuracy, $\tau_{dm} \le \tau_{max}$ is the maximum dynamic delay-time range over which ACF exponential behavior is modeled for Brownian motion with a given accuracy.

In our optimization, the reference point is taken inside the decay time τ^* range:

$$\frac{\tau_r}{\tau^*} = \frac{2}{3} \tag{59}$$

and the maximum dynamic range of the delay time is found from

$$\left| \frac{\mathrm{RDC}\left(\frac{\tau_{dm}}{\tau^*}, \varphi \to 0\right)}{\mathrm{RDC}\left(\frac{\tau_r}{\tau^*}, \varphi \to 0\right)} - 1 \right| \le \epsilon \tag{60}$$

C. Optimization of the Displacement Parameter. The dependency of systematic error and maximum dynamic range of delay time on the squared displacement parameter f^2 are given in Figures 3 and 4, respectively. Calculations are carried out for the parameters listed in Table 2 and for the calculation accuracy $\epsilon = 0.1$. Only one numerical generator, ran(*idum*), is taken for the generation of all random parameters.

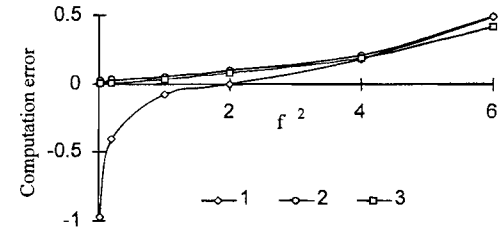

Figure 3. Dependency of the systematic error $\epsilon_a(\tau_r/\tau^* = 2/3)$ (see eqs 14 and 52) of the numerical model on the squared displacement parameter. Curves 1–3 correspond to $\{N_p = 1, T = 80\}$, $\{N_p = 10, T = 800\}$, and $N_p = 100, T = 8000\}$, respectively. $N_q = 3$ for all curves.

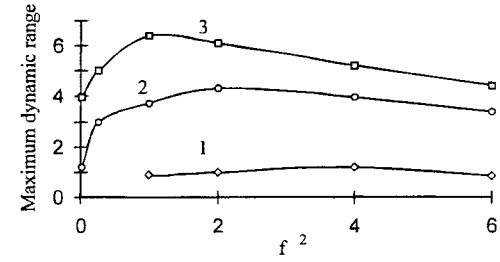

Figure 4. Maximum dynamic range τ_{dm}/τ^* (see eq 60) of the numerical technique for ACF modeling vs the squared displacement parameter. The error ϵ used for the estimation of this range by eq 60 is equal to 0.1. $N_q = 3$ for all curves. Curve 1 corresponds to $\{N_p = 1, T = 80\}$; curve 2 corresponds to $\{N_p = 10, T = 800\}$; curve 3 corresponds to $\{N_p = 100, T = 8000\}$.

Table 2. Parameters Taken for the Analysis of Systematic Error and Maximum Dynamic Delay-Time Range in ACF Numerical Modeling

f^2	N_τ	n
0.01	16	400
0.25	16	16
1	16	4
2	16	2
4	16	1
6	12	1

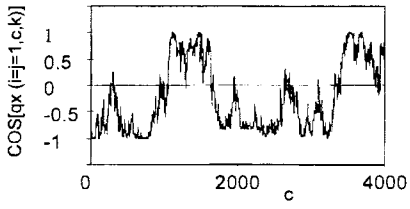

Figure 5. An integrated function $\cos[qx(i=j=1, c, k)]$ in eq 49 vs the discrete time c for the displacement parameter $f = 0.1$: $n = 400$, $m = 7$ ($k = 2800$), $N_p = 1$.

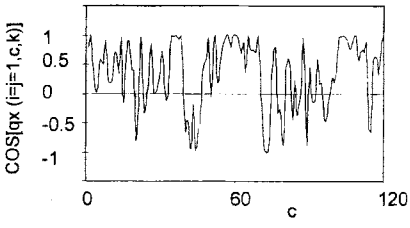

Figure 6. An integrated function $\cos[qx(i=j=1, c, k)]$ in eq 49 vs the discrete time c for the displacement parameter $f = 1$: $n = 4$, $m = 7$ ($k = 28$), $N_p = 1$.

The systematic error and the reduction of the dynamic delay-time range are caused, in general, by oscillations of the integrated functions $\cos[qh(i, j=i, c, k)]$ and $\sin[qh(i, j=i, c, k)]$ in eq 49 (see also ref 1, p 103). As follows from the analysis of the above functions presented in Figures 5 and 6 for an arbitrary ith single-moving particle, the period of the low-frequency oscillations is approximately k for $f = 0.1$ and is several times k for $f = 1$.

Hence, acceptable calculation accuracy for a single-moving particle can be achieved if the upper time range of integration, T, is greater than the period of low-frequency oscillations mentioned above. An insufficient magnitude of the upper range of integration leads to incorrect results (see Figures 3 and 5, curve 1, at $f < 0.5$).

The period of high oscillations is 5−10 for $f = 0.1-1$, and their amplitude increases relative to the low-frequency amplitude with an increase of the displacement parameter f. These oscillations cause an increase in systematic error (especially, for $f^2 > 2$) and a decrease of the dynamic range for greater values of f.

Curve 3 in Figure 3, obtained for a large upper range of integration, can be used to estimate the limiting systematic error of the model, generally caused by numerical errors in the integration of oscillated functions.

An analysis of Figures 3 and 5 shows that the range $0.8 < f^2 < 1.5$ fits optimization criteria presented by eq 57. For further investigations, $f = 1$ is chosen as an optimal displacement parameter.

D. Optimization of M, n, and N_τ Parameters. Additional investigations performed in order to optimize other parameters of the model indicated that decreasing the number of particle-ensembles up to $N_c = 216$, the set $\{M = 25, n = 2, N_\tau = 16\}$ satisfactorily meets well all three of the above-mentioned optimization criteria.

Thus, the numerical model, characterized by optimized parameters $\{f = 1, M = 25, n = 2, N_\tau = 16\}$, is prepared for the investigation of the multiple-scattering (MLS) effect. Figures 7 and 8 illustrate the systematic errors of the model, which arise at the stage of generation of particle dynamics and ACF modeling, respectively. An additional average over $idum = -3, -5$, and -7 is used. A further increase in accuracy was achieved by applying a set of new random numerical generations (an individual generator for each random parameter of the model in Figures 7 and 8, instead of one generator for all random parameters, as in Figures 3 and 4).

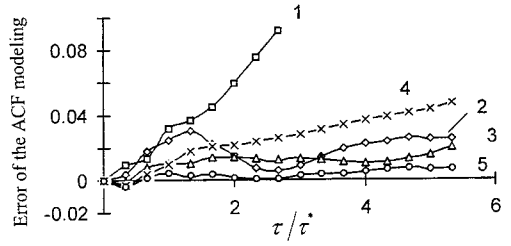

Figure 7. Systematic errors $\epsilon_a(\tau/\tau^*)$ (see eqs 14 and 52) of the ACF modeling for the different number of free particle vs the relative discrete delay time. An additional average is provided over three different histories of ensemble generation ($idum = \{-3, -5, -7\}$). $M = 25$, $n = 2$, $N_\tau = 16$. Curves 1−5 correspond to 3, 5, 10, 25, and 50 spheres in an ensemble.

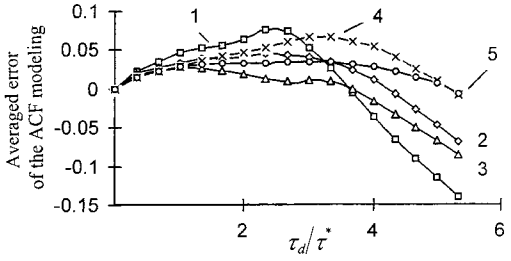

Figure 8. Averaged error $\langle\epsilon_a(\tau_d)\rangle$ (see eqs 15 and 53) of the ACF modeling vs the relative average interval τ_d/τ^* for different numbers of particles in particle-ensembles. An additional average is provided over three different histories of ensemble generation ($idum = \{-3, -5, -7\}$). $M = 25$, $n = 2$, $N_\tau = 16$. Curves 1−5 correspond to 3, 5, 10, 25, and 50 spheres in an ensemble.

Figures 7 and 8 show that by generation of only $N_c = 216$ particle-ensembles and $N_p = 5$ (or more) particles, the proposed technique allows modeling of free-particle dynamics and ACF, with error less than 4−6% in the range of delay time $\tau/\tau^* < 5$.

The model can be used for estimating the effect of multiple scattering, even if the number of spheres in an ensemble is limited by $N_p = 3$, when both errors are less than 4%, if $\tau/\tau^* \leq 1$.

4. Modeling of the Effect of Multiple Scattering on the ACF. Some calculation results are presented below to show the practical application of the numerical model which has been developed. The model and obtained results appear to be among the ground-breaking rigorous theoretical investigations of the influence of multiple scattering by interacting particles on the measurement properties of highly concentrated systems in photon correlation spectroscopy (PCS).

Calculations are provided for the depolarized component of the backscattered electric field (i.e., $\theta_s = 180°$). We restrict this presentation by the depolarized component of the scattered electric field (with polarization perpendicular to the incident-wave polarization), because this component is absent for the scattering from a single sphere ($N_p = 1$) and it depends strongly on the multiple scattering from the ensemble of spheres ($N_p > 1$). The wavelength of the x-polarized incident plane wave is 0.6328 μm. The

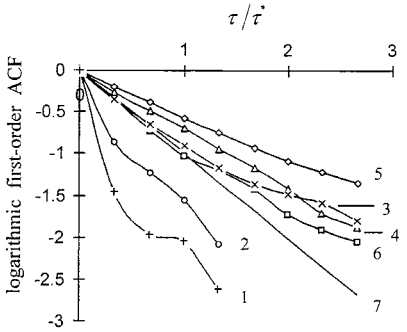

Figure 9. Modeling of the influence of multiple scattering from five interacting spheres on the logarithmic first-order ACF of the depolarized component of the scattered electric field for different sphere diameters. Volume fraction $\varphi = 0.05$. Curves 1−5 correspond to 41-, 63-, 115-, 199-, and 326-nm spheres, respectively, and to the rigorous simulations of multiple scattering by eqs 39 and 44. Curve 6 corresponds to self-diffusion assumption for a set of five Brownian particles simulated by eq 49. Curve 7 corresponds to an ideal Brownian system (see eq 7).

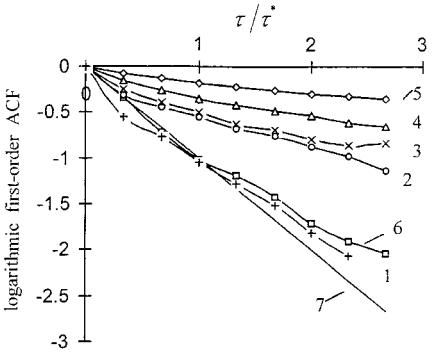

Figure 10. Modeling of the influence of multiple scattering from five interacting spheres on the logarithmic first-order ACF of the depolarized component of the scattered electric field for different sphere diameters: curves 1−5 correspond to 41-, 63-, 115-, 119-, and 326-nm spheres, respectively, and to the rigorous simulations of multiple scatterings by eqs 39 and 44. Curve 6 corresponds to the self-diffusion assumption for a set of five Brownian particles simulated by eq 49. Curve 7 corresponds to an ideal Brownian system (see eq 7). Volume fraction $\varphi = 0.45$.

complex refractive index of spheres, $1.59-i0$, the refractive index of the solvent (water), $1.33-i0$, and the magnitudes 326,199, 115, 63, and 41 nm of spheres diameter are taken to be identical to the dispersion parameters comprehensively investigated experimentally by a fiber optic sensor in ref 14. Other main parameters of the numerical model are $\{M = 25, n = 2, N_\tau = 16, f = 1, idum = -3\}$.

Modeling of the effect of multiple scattering on the ACF as a function of the diameter of the spherical particles is given in Figures 9 and 10 for the volume fraction of suspended spheres 0.05 and 0.45, respectively. One can check that the parameter $f = 1$, optimized for Brownian motion, satisfies also eq 34 over the fully investigated range of volume fraction. In the figures, the logarithmic ACF is defined by $\ln|g^{(1)}(\tau)|$.

Lines 7 plotted in Figures 9 and 10 reflect an exponential behavior of the autocorrelation function of the light scattered by an ideal Brownian system (see eq 7). Curve 6 marked by □ corresponds to the self-diffusion assumption for a set of five Brownian particles simulated by eq 49. Deviation of this curve from the line is caused by the calculation error because of the small number of Brownian particles ($N_p = 5$). The error $\epsilon_a(\tau)$ of the ACF estimation is negligible (less than 1.35%) for the range of the relative discrete delay time $\tau/\tau^* < 1.4$. Deviations of other curves

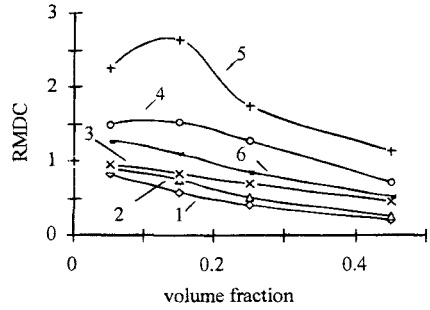

Figure 11. Contribution of multiple scattering by three interacting spheres on the relative diffusion coefficient, RMDC, for different volume fractions and the diameter of spheres. RMDC is extracted from the ACF model of the depolarized component of the scattered electric field. The range of averaging is $\tau_d/\tau^* = 1$. Curves 1−5 correspond to 41-, 63-, 115-, 199-, and 326-nm spheres, respectively. Curve 6 corresponds to the 90-nm sphere.

in the same range $\tau/\tau^* < 1.4$ demonstrate the contribution of the multiple scattering by five interacting spheres on the ACF. As may be seen from Figures 9 and 10, the numerical model allows for the prediction of the contribution of multiple scattering (MLS) as a function of the sphere's diameter and the volume fraction.

Dependency of the relative diffusion coefficient, RMDC, which is extracted form the ACF modeled for the depolarized component of the scattered electric field, is presented in Figure 11 versus the volume fraction for three interacting spheres only. Averaging of $\langle \ln|g^{(1)}(\tau)| \rangle$ is provided over the dynamic range $\tau_d/\tau^* = 1$, where the numerical error is less than 4% for Brownian free particles (see also Figure 9, curves 6 and 7). Calculation results are reproducible: an additional averaging over $idum = -3, -5$, and -7 (in other words, over three sets of particle-ensembles with different histories of particle motion) was performed for more accurate modeling of some parts of simulated data only. Figures 9−11 show general tendencies of the ACF distortion by multiple-scattering effects when the depolarized component of the scattered electric field is modeled. These tendencies are reproducible even if the number of modeled particles is small ($N_p = 3-5$).

5. Conclusions

A numerical model is proposed as a tool for the study of multiple-scattering effects in PCS measurements. Limitation on the number of particles in an ensemble and on the number of particle-ensembles (which are used to model the motion of particles) is necessary to create an effective code, but these limitations lead to a decrease in accuracy of any numerical technique. In this work, the accuracy of the proposed technique, characterized by systematic error and by dynamic delay-time range, is investigated for Brownian free particles. Two discrete time scales are used for the modeling of particle interactions and for numerical ACF simulation in order to economize the computation time. It is shown that the systematic error of the ACF calculation and the reduction of the dynamic delay-time range are caused by the low- and high-frequency oscillations of the integrated functions.

For a single-moving particle, acceptable calculation accuracy can be accomplished if the upper time range T of the integration by eq 44 is larger than the period of the low-frequency oscillations. The period of the low-frequency oscillations is about equal to the relative delay time k for the displacement parameter $f = 0.1$ and is roughly several times k for $f = 1$. An insufficient upper range magnitude leads to incorrect results (see Figures

3 and 4, curve 1, at $f < 0.5$). The high-frequency oscillations cause a decrease in the dynamic delay-time range and an increase in the systematic error for larger values of f (especially, for $f^2 > 2$).

In the optimized numerical model, characterized by a set of parameters $\{f = 1, M = 25, n = 2, N_\tau = 16\}$, the maximum calculation error of the ACF estimator is suppressed up to 4% for the limited number of particle-ensembles $N_c = 216$ and the number of particles $N_p = 3$ if $\tau/\tau^* \leq 1$ (see Figure 8, curve 1). Hence, even in the case for strong limitations ($N_c = 216$, $N_p = 3$), the numerical model allows for prediction of a multiple-scattering contribution of 4% (and more) to the PCS results. Furthermore, multiple-scattering contribution of less than 4% can also be predicted, if the signs of this contribution and the calculation error are opposite.

Modeling of the ACF distortion, provided for the depolarized electric field scattered by a small number of particles, $N_p = 3-5$, shows efficiency of the proposed technique for investigation of the multiple-scattering effects in PCS. More comprehensive investigation of the multiple-scattering effects by large number of particles and modeling of suppression of these effects by one-beam cross correlation are discussed in another paper.[28]

Acknowledgment. The assistance of M. Weckx in administrative support, of L. Deriemaekeris in engineering support, and of Y. De Smet in comprehensive discussions is greatly appreciated. V. I. Ovod is grateful to the Brussels-Capital Region and the Ministry of Economic Affairs, Belgium, for financial support of this work.

LA962130K